3D buckling analysis of FGM sandwich plates under bi-axial compressive loads

Chih-Ping Wu[*] and Wei-Lun Liu

Department of Civil Engineering, National Cheng Kung University, Tainan 70101, Taiwan, ROC

Abstract. Based on the Reissner mixed variational theorem (RMVT), finite rectangular layer methods (FRLMs) are developed for the three-dimensional (3D) linear buckling analysis of simply-supported, fiber-reinforced composite material (FRCM) and functionally graded material (FGM) sandwich plates subjected to bi-axial compressive loads. In this work, the material properties of the FGM layers are assumed to obey the power-law distributions of the volume fractions of the constituents through the thickness, and the plate is divided into a number of finite rectangular layers, in which the trigonometric functions and Lagrange polynomials are used to interpolate the in- and out-of-plane variations of the field variables of each individual layer, respectively, and an *h*-refinement process is adopted to yield the convergent solutions. The accuracy and convergence of the RMVT-based FRLMs with various orders used for expansions of each field variables through the thickness are assessed by comparing their solutions with the exact 3D and accurate two-dimensional ones available in the literature.

Keywords: Reissner's mixed variational theorem; computational modeling; finite layer methods; functionally graded materials; buckling; plates

1. Introduction

The buckling of sandwiched rectangular flat plates composed of fiber-reinforced composite materials (FRCMs) or functionally graded materials (FGMs) has attracted considerable attention for several decades, since this is one of the main failures that occur in these structures, which are widely applied in areas such as the aircraft, civil engineering and ship-building industries. Moreover, many comprehensive reviews of literature on the various computational models used for multilayered FRCM/FGM structures have been carried out (Noor and Burton 1990, Reddy 1993, Noor *et al*. 1996, Carrera 2000a, b, 2001, 2003a, Carrera and Ciuffreda 2005a, Wu and Chen 2008, Wu *et al*. 2008, Carrera and Brischetto 2009).

Some two-dimensional (2D) plate theories have been proposed and applied to this subject, such as the equivalent single-layered theories (ESLTs), layerwise (or so-called discrete layer) theories, and zig-zag theories. Reddy and Phan (1985) and Wu and Chen (1994) developed the global and local higher-order shear deformation theories (HSDTs) for the stability analysis of isotropic, orthotropic and laminated plates, respectively, in which the global higher-order displacement

---

*Corresponding author, Professor, E-mail: cpwu@mail.ncku.edu.tw

model and layerwise one were assumed, and in the latter the displacement continuity conditions were introduced to the potential energy functional of the plates using the Lagrange multiplier method and were satisfied using a generalized variational principle. A global-local HSDT theory was also proposed for the buckling analysis of laminated composite and sandwich plates under mechanical and thermal loads by Wu and Chen (2007) and Wu *et al*. (2008). Kim *et al*. (2009a) and Thai and Kim (2011) studied the buckling of isotropic and orthotropic plates using a two-variable refined plate theory (Kim *et al*. 2009b), in which the transverse shear effects were considered without using the shear correction factor. Using a sinusoidal shear deformation theory, Zenkour (2005) carried out a comprehensive buckling analysis of FGM sandwich plates. Zhao *et al*. (2009) applied a first-order shear deformation theory (FSDT), combined with the element-free *kp*-Ritz method, to the buckling analysis of FGM plates under thermo-mechanical loads. Reddy and Khdeir (1989) presented a comparative study of the analytical and finite-element solutions for the buckling of laminated cross-ply plates with various boundary conditions using the classical, first-order, and third-order laminate theories.

In addition to the above-mentioned theories, which are based on the principle of virtual displacement (PVD), Reissner (1984, 1986a, b) proposed an alternative variational principle, known as Reissner's mixed variational theorem (RMVT), for the analysis of laminated structures. In the former approaches, the displacement components are regarded as the primary field variables subject to variation, while both the displacement and transverse stress components are regarded as these in the RMVT. A review of the literature on using the RMVT for analyses of various laminated beams, plates and shells was undertaken by Carrera (2001). Zenkour and Fares (2001) and Zenkour and Al-Sheikh (2001) undertook a comparative study of the bending, buckling and free vibration problems associated with cylindrical shells made of nonhomogeneous materials using a variety of simple and mixed shear deformation theories, and presented analytical solutions for critical load parameters with assorted boundary conditions. Based on the PVD and RMVT, Carrera (2003b) developed a unified formulation to assess the performance of a variety of plate theories for the bending (Carrera and Ciuffreda 2005b) and buckling (Nali *et al*. 2011) analyses of laminated composite plates, and it has been concluded that the RMVT-based theories have better performance than the PVD-based ones for assorted analyses of multilayered structures, and thus the RMVT should be considered a natural tool for the analysis of multilayered structures, similar to how the PVD is used for isotropic single-layer ones.

Some exact and approximate three-dimensional (3D) methods have also been presented for this subject. Noor (1975) presented the 3D buckling solutions for a wide range of lamination and geometric parameters, in which a quantitative assessment was made for the accuracy and range of validity of the classical and shear deformation plate theories. Within the framework of 3D elasticity theory, Fan and Ye (1993) derived the state space equations of the buckling of orthotropic thick plates without imposing any kinetic and kinematics assumptions in the formulation, and obtained a unified exact solution for the buckling of simply-supported rectangular laminates by the Cayley-Hamilton theorem. Gu and Chattopadhyay (2000) presented the 3D exact solutions for the buckling of simply-supported, laminated orthotropic plates under uni-axial compressive loads, in which a uniform pre-buckling stress assumption was made. Cheung and Kong (1993) proposed a global–local approach for the approximate 3D bending, vibration and buckling analyses of rectangular thick laminated plates, in which the cross-section of a laminated plate was discretized into conventional eight-node elements, and a cubic B3-spline function was used to interpolate the field variables in the length direction. Teo and Liew (1999a, b) applied the differential quadrature method (DQM) to the 3D bending, free vibration and buckling analyses of rectangular plates.

Referring to Carrera's unified formulation (CUF) and combining it with a variable kinematics model, D'Ottavio and Carrera (2010) developed an RMVT-based discrete layer theory for the linearized buckling analysis of laminated and shells. Na and Kim (2004, 2006) presented the approximate 3D solutions for the buckling of FGM plates under thermo-mechanical loads, in which the material properties were assumed to be temperature dependent, a conventional eighteen-node solid element was used to model the plates in the spatial coordinates, and the Crank-Nicolson method was used for a time discretization. Based on the perturbation method, Wu and Chen (2001) and Wu and Chiu (2001, 2002) presented the 3D asymptotic solutions for the elasto-static, thermally induced static and dynamic buckling of multilayered anisotropic conical shells.

Building on the PVD, Cheung and Jiang (2001) developed the finite rectangular layer methods (FRLMs) to study the 3D static problems of simply-supported, piezoelectric composite laminates, in which the displacement and electric potential components were regarded as the primary variables subject to variation. Subsequently, Akhras and Li (2007, 2008) applied these PVD-based FRLMs to the 3D static, vibration, stability and thermal buckling analyses of piezoelectric composite plates. Because it has been reported that the RMVT-based theories are superior to the PVD-based ones for the analysis of multilayered structures (Carrera *et al*. 2008, 2010, Brischetto and Carrera 2010), Wu and Li (2010) and Wu and Chang (2012) developed the unified formulations of RMVT-based FRLMs and RMVT-based finite cylindrical layer methods (FCLMs) for the bending analysis of multilayered FGM plates and cylinders, respectively. Implementing these methods in the cases of FRCM/FGM plates and cylinders shows that the convergence is rapid and their convergent solutions are in excellent agreement with the exact 3D ones available in the literature.

In this article, the RMVT-based FRLMs are extended to the 3D elasto-static buckling analysis of multilayered (or sandwiched) FRCM/FGM plates under bi-axial compressive loads, in which the linear buckling theory is used, the material properties of the FGM layer are assumed to obey the power-law distributions of the volume fraction of the constituents through the thickness coordinate, and the orders used for expansions of displacement components and transverse stress ones through the thickness coordinate are taken to be identical to one another, which are 1, 2 and 3. The deviations of the present solutions obtained using two different sets of the initial membrane stresses, based on the uniform strain assumption and the uniform stress one, are examined, and those between the present solutions obtained using von Kʹarmʹan's approximations and full kinematic nonlinearity are also evaluated. A parametric study with regard to some crucial effects on the critical load parameters of the multilayered FRCM/FGM plates is carried out, such as the length-to-width, length-to-thickness, orthotropic and load intensity ratios, and the material-property gradient index.

2. Pre-buckling state in a multilayered FGM plate

We consider a simply-supported, multilayered FGM plate subjected to bi-axial compression, the intensities (or corresponding loads) of which are p_x (or P_x) and p_y (or P_y) applied at the y-ζ and x-ζ planes, respectively, as shown in Fig. 1(a), and $p_y = k_p\, p_x$, $P_x = p_x\, L_y$ and $P_y = p_y\, L_x$, in which k_p denote the load intensity ratio, and $0 \le k_p \le 1$, and L_x and L_y denote the in-plane dimensions in the x and y directions. A Cartesian global coordinate system (x, y and

ζ coordinates) is located on the middle plane of the plate, and a set of Cartesian local thickness coordinates, z_m ($m = 1, 2, 3, \cdots, N_l$), is located at the mid-plane of each individual layer, as shown in Fig. 1(b), where N_l is the total number of the layers constituting the plate. The thicknesses of each individual layer and the plate are h_m ($m = 1, 2, \cdots, N_l$) and h, respectively, while $h = \sum\limits_{m=1}^{N_l} h_m$.

The relationship between the global and local thickness coordinates in the mth-layer is $\zeta = \bar{z}_m + z_m$, in which $\bar{z}_m = (\zeta_m + \zeta_{m-1})/2$, and ζ_m and ζ_{m-1} are the global thickness coordinates measured from the mid-plane of the plate to the top and bottom surfaces of the mth-layer, respectively.

In this paper, the 3D linear buckling theory is used to derive the buckling of multilayered FGM plates, in which a set of membrane state of stresses exist in the plate just before instability occurs. Based on the uniform strain assumption, the displacement components of the mth-layer at the initial position are given by

$$\bar{u}_x^{(m)} = A_o \, x, \qquad \bar{u}_y^{(m)} = B_o \, y, \qquad \text{and} \qquad \bar{u}_\zeta^{(m)} = W_o(\zeta) \qquad m = 1, 2, \cdots, N_l \qquad \text{(1a-c)}$$

where A_o and B_o are a certain arbitrary constants, and these will be determined later in this paper by means of satisfying the force equilibrium equation in the x and y directions at the edges.

According to the initial displacement model given in Eq. (1), it is assumed that in the pre-buckling state the plate is free of initial shear stresses (i.e., $\bar{\tau}_{x\zeta}^{(m)} = \bar{\tau}_{y\zeta}^{(m)} = \bar{\tau}_{xy}^{(m)} = 0$, $m = 1, 2, \cdots, N_l$), and the initial normal stresses in the mth-layer can be expressed as

$$\bar{\sigma}_x^{(m)} = Q_{11}^{(m)} A_o + Q_{12}^{(m)} B_o , \quad \bar{\sigma}_y^{(m)} = Q_{12}^{(m)} A_o + Q_{22}^{(m)} B_o , \text{ and } \bar{\sigma}_\zeta^{(m)} = 0 \quad m = 1, 2, \cdots, N_l \qquad \text{(2a-c)}$$

where $Q_{ij}^{(m)} = c_{ij}^{(m)} - \left(c_{i3}^{(m)} c_{j3}^{(m)} / c_{33}^{(m)} \right)$ ($i, j = 1, 2$), and both the stress equilibrium equations in x, y and ζ directions in the plate domain and the loading conditions on the top and bottom surfaces

Taking a free body diagram at each edge, we can express the force equilibrium equations in the x direction at the edges $x = 0$ and $x = L_x$, and in the y direction at $y = 0$ and $y = L_y$, as follows

$$L_y \int_{-h/2}^{h/2} \bar{\sigma}_x^{(m)}(\zeta) d\zeta = -P_x , \qquad \text{and} \qquad L_x \int_{-h/2}^{h/2} \bar{\sigma}_y^{(m)}(\zeta) d\zeta = -P_y \qquad \text{(3a, b)}$$

in which $P_y = k_p \left(L_x / L_y \right) P_x$.

Substituting Eqs. (2(a)-2(c)) in Eqs. (3(a) and 3(b)) yields

$$A_0 = -S_x \, P_x , \qquad \text{and} \qquad B_0 = -S_y \, P_x \qquad \text{(4a, b)}$$

where $S_x = \left[(A_{22} / L_y) - (k_p \, A_{12} / L_y) \right] / \left[A_{11} \, A_{22} - (A_{12})^2 \right]$,

$\qquad S_y = \left[(k_p A_{11} / L_y) - (A_{12} / L_y) \right] / \left[A_{11} \, A_{22} - (A_{12})^2 \right]$,

in which $A_{ij} = \sum\limits_{m=1}^{N_l} \int_{\zeta_{m-1}}^{\zeta_m} Q_{ij}^{(m)} \, d\zeta$, and $i, j = 1$ and 2.

Using Eqs. (2(a)-2(c)) and Eqs. (4(a) and 4(b)), we may determine the pre-buckling state of stresses in the plate as follows

$$\overline{\sigma}_x^{(m)} = -\overline{f}_x^{(m)} P_x, \quad \text{and} \quad \overline{\sigma}_y^{(m)} = -\overline{f}_y^{(m)} P_x \qquad (5a, b)$$

where $\overline{f}_x^{(m)}$ and $\overline{f}_y^{(m)}$ denote the influence functions of the pre-buckling membrane stresses of the mth-layer of the plate under bi-axial compressive loads, and $\overline{f}_x^{(m)} = Q_{11}^{(m)} S_x + Q_{12}^{(m)} S_y$ and $\overline{f}_y^{(m)} = Q_{12}^{(m)} S_x + Q_{22}^{(m)} S_y$.

The above-mentioned membrane stresses will be regarded as the initial stresses of the plate, and are introduced in the formulation corresponding to the perturbed state of the plate.

3. Perturbed state in a multilayered FGM plate

In this paper, we aim at extending the early RMVT-based FRLMs (Wu and Li 2010) to the 3D buckling analysis of simply-supported, multilayered FGM and FRCM plates under bi-axial compressive loads, and the detailed derivation of the formulation is described in the following subsections.

3.1 The kinematic and kinetic assumptions

Based on the use of 3D linear buckling theory, a set of membrane stresses given in Eqs. (5(a) and 5(b)) is assumed to exist in the plate just before instability occurs, and this is regarded as the initial state of stresses, which is introduced in Reissner's energy functional of the multilayered FGM plate, in which the incremental stresses associated with the small incremental displacements perturbed from the state of neutral equilibrium will be considered.

A discrete layer model with either linear, quadratic or cubic function distributions through the thickness coordinate for the incremental displacements is adopted as the kinematic field of the mth-layer of the plate in this formulation, of which the domain is in $0 \le x \le L_x$, $0 \le y \le L_y$ and $(-h_m/2) \le z_m \le (h_m/2)$, and is given by

$$u_x^{(m)}(x, y, z_m) = \sum_{i=1}^{n_u+1} \left[\psi_u^{(m)}(z_m)\right]_i \left[u^{(m)}(x, y)\right]_i \qquad (6)$$

$$u_y^{(m)}(x, y, z_m) = \sum_{i=1}^{n_u+1} \left[\psi_u^{(m)}(z_m)\right]_i \left[v^{(m)}(x, y)\right]_i \qquad (7)$$

$$u_\zeta^{(m)}(x, y, z_m) = \sum_{j=1}^{n_w+1} \left[\psi_w^{(m)}(z_m)\right]_j \left[w^{(m)}(x, y)\right]_j \qquad (8)$$

where ($u_x^{(m)}$, $u_y^{(m)}$, $u_\zeta^{(m)}$) denote the incremental displacement components of the mth-layer of the plate in the x, y and ζ directions, respectively; $\left(u^{(m)}\right)_i$, $\left(v^{(m)}\right)_i$, $\left(w^{(m)}\right)_j$ with $(i = 1, 2, \cdots, n_u + 1)$ and $(j = 1, 2, \cdots, n_w + 1)$ are the incremental displacement components at the nodal planes of the mth-layer of the plate; and $\left(\psi_u^{(m)}\right)_i$ $(i = 1, \cdots, n_u + 1)$ and $\left(\psi_w^{(m)}\right)_j$ $(j = 1, 2, \cdots, n_w + 1)$ are the corresponding shape functions, in which n_u and n_w denote the related orders used for the expansion of the in- and out-of-plane incremental displacements, respectively.

The incremental transverse shear and normal stresses are also regarded as the primary variables in these RMVT-based FRLMs, and are assumed as follows

$$\tau_{x\zeta}^{(m)}(x,y,z_m) = \sum_{i=1}^{n_\tau+1} \left[\psi_\tau^{(m)}(z_m)\right]_i \left[\tau_{13}^{(m)}(x,y)\right]_i \tag{9}$$

$$\tau_{y\zeta}^{(m)}(x,y,z_m) = \sum_{i=1}^{n_\tau+1} \left[\psi_\tau^{(m)}(z_m)\right]_i \left[\tau_{23}^{(m)}(x,y)\right]_i \tag{10}$$

$$\sigma_\zeta^{(m)}(x,y,z_m) = \sum_{j=1}^{n_\sigma+1} \left[\psi_\sigma^{(m)}(z_m)\right]_j \left[\sigma_3^{(m)}(x,y)\right]_j \tag{11}$$

where $\left(\tau_{13}^{(m)}\right)_i$, $\left(\tau_{23}^{(m)}\right)_i$, $\left(\sigma_3^{(m)}\right)_j$ in which $(i=1,2,\cdots,n_\tau+1)$ and $(j=1,2,\cdots,n_\sigma+1)$ are the transverse stress components at the nodal planes of the mth-layer of the plate; and $\left(\psi_\tau^{(m)}\right)_i$ $(i=1,2,\cdots,n_\tau+1)$ and $\left(\psi_\sigma^{(m)}\right)_i$ $(i=1,2,\cdots,n_\sigma+1)$ are the corresponding shape functions in which n_τ and n_σ denote the related orders used for the expansion of the incremental transverse shear and normal stresses, respectively.

The linear constitutive equations for the mth-layer of the plate, which are valid for the orthotropic materials, are given by

$$\begin{Bmatrix} \sigma_x^{(m)} \\ \sigma_y^{(m)} \\ \sigma_\zeta^{(m)} \\ \tau_{y\zeta}^{(m)} \\ \tau_{x\zeta}^{(m)} \\ \tau_{xy}^{(m)} \end{Bmatrix} = \begin{bmatrix} c_{11}^{(m)} & c_{12}^{(m)} & c_{13}^{(m)} & 0 & 0 & 0 \\ c_{12}^{(m)} & c_{22}^{(m)} & c_{23}^{(m)} & 0 & 0 & 0 \\ c_{13}^{(m)} & c_{23}^{(m)} & c_{33}^{(m)} & 0 & 0 & 0 \\ 0 & 0 & 0 & c_{44}^{(m)} & 0 & 0 \\ 0 & 0 & 0 & 0 & c_{55}^{(m)} & 0 \\ 0 & 0 & 0 & 0 & 0 & c_{66}^{(m)} \end{bmatrix} \begin{Bmatrix} \varepsilon_x^{(m)} \\ \varepsilon_y^{(m)} \\ \varepsilon_\zeta^{(m)} \\ \gamma_{y\zeta}^{(m)} \\ \gamma_{x\zeta}^{(m)} \\ \gamma_{xy}^{(m)} \end{Bmatrix} \tag{12}$$

where $(\sigma_x^{(m)}, \sigma_y^{(m)}, \cdots, \tau_{xy}^{(m)})$ are the incremental stress components; $(\varepsilon_x^{(m)}, \varepsilon_y^{(m)}, \cdots, \gamma_{xy}^{(m)})$ are the incremental strain components; and $c_{ij}^{(m)}$ are the stiffness coefficients, which are constants through the thickness coordinate in the homogeneous elastic layers, and variable through the thickness coordinate in the FGM layers (i.e., $c_{ij}^{(m)}(\zeta)$).

The incremental strain components of each individual layer based on the assumed incremental displacement model in Eqs. (6)-(8) are written in the following form

$$\begin{aligned} \varepsilon_x^{(m)} &= u_x^{(m)},_x \\ &= \sum_{i=1}^{n_u+1} \left(\psi_u^{(m)}\right)_i u_i^{(m)},_x \end{aligned} \tag{13}$$

$$\begin{aligned} \varepsilon_y^{(m)} &= u_y^{(m)},_y \\ &= \sum_{i=1}^{n_u+1} \left(\psi_u^{(m)}\right)_i v_i^{(m)},_y \end{aligned} \tag{14}$$

$$\varepsilon_{\zeta}^{(m)} = u_{\zeta}^{(m)},_{\zeta}$$

$$= \sum_{j=1}^{n_w+1} \left(D\psi_w^{(m)} \right)_j w_j^{(m)} \tag{15}$$

$$\gamma_{x\zeta}^{(m)} = u_x^{(m)},_{\zeta} + u_{\zeta}^{(m)},_x$$

$$= \sum_{i=1}^{n_u+1} \left(D\psi_u^{(m)} \right)_i u_i^{(m)} + \sum_{j=1}^{n_w+1} \left(\psi_w^{(m)} \right)_j w_j^{(m)},_x \tag{16}$$

$$\gamma_{y\zeta}^{(m)} = u_y^{(m)},_{\zeta} + u_{\zeta}^{(m)},_y$$

$$= \sum_{i=1}^{n_u+1} \left(D\psi_u^{(m)} \right)_i v_i^{(m)} + \sum_{j=1}^{n_w+1} \left(\psi_w^{(m)} \right)_j w_j^{(m)},_y \tag{17}$$

$$\gamma_{xy}^{(m)} = u_x^{(m)},_y + u_y^{(m)},_x$$

$$= \sum_{i=1}^{n_u+1} \left(\psi_u^{(m)} \right)_i u_i^{(m)},_y + \sum_{i=1}^{n_u+1} \left(\psi_u^{(m)} \right)_i v_i^{(m)},_x \tag{18}$$

in which the commas denote partial differentiation with respect to the suffix variables;

$$D\psi_k^{(m)} = \frac{d\psi_k^{(m)}}{dz_m} \quad (k = u, \ w, \ \tau \ \text{and} \ \sigma).$$

3.2 The Reissner mixed variational theorem

The Reissner mixed variational theorem is used to derive the equilibrium equations at the perturbed state of the plate for the RMVT-based FRLMs, and its corresponding energy functional of the plate perturbed from the neutral equilibrium state is written in the form of

$$\Pi_R = \sum_{m=1}^{N_l} \int_{-h_m/2}^{h_m/2} \iint_{\Omega} \left[\sigma_x^{(m)} \varepsilon_x^{(m)} + \sigma_y^{(m)} \varepsilon_y^{(m)} + \sigma_{\zeta}^{(m)} \varepsilon_{\zeta}^{(m)} + \tau_{x\zeta}^{(m)} \gamma_{x\zeta}^{(m)} + \tau_{y\zeta}^{(m)} \gamma_{y\zeta}^{(m)} + \tau_{xy}^{(m)} \gamma_{xy}^{(m)} - B\left(\sigma_{ij}^{(m)} \right) \right]$$

$$dx \, dy \, dz_m$$

$$- \sum_{m=1}^{N_l} \iint_{\Omega} (P_x) \left[\bar{f}_x^{(m)} \hat{\varepsilon}_x^{(m)} + \bar{f}_y^{(m)} \hat{\varepsilon}_y^{(m)} \right] dx \, dy \, dz_m - \int_{-h_m/2}^{h_m/2} \int_{\Gamma_{\sigma}} \left(\bar{t}_x^{(m)} u_x^{(m)} + \bar{t}_y^{(m)} u_y^{(m)} + \bar{t}_{\zeta}^{(m)} u_{\zeta}^{(m)} \right) d\Gamma \, dz_m \tag{19}$$

$$- \int_{-h_m/2}^{h_m/2} \int_{\Gamma_u} \left[(u_x^{(m)} - \bar{u}_x^{(m)}) t_x^{(m)} + (u_y^{(m)} - \bar{u}_y^{(m)}) t_y^{(m)} + (u_{\zeta}^{(m)} - \bar{u}_{\zeta}^{(m)}) t_{\zeta}^{(m)} \right] d\Gamma \, dz_m$$

where Ω denotes the plate domain on the $x-y$ plane; Γ_{σ} and Γ_u denote the portions of the edge boundary, where the surface traction and displacement components (i.e., $\bar{t}_i^{(m)}$, $\bar{u}_i^{(m)}$ in which $i = x, \ y$ and ζ) are prescribed, respectively; $B(\sigma_{ij}^{(m)})$ is the complementary density function, and $\partial B(\sigma_{ij}^{(m)})/\partial \sigma_{ij} = \varepsilon_{ij}$; $\hat{\varepsilon}_x^{(m)}$ and $\hat{\varepsilon}_y^{(m)}$ denote the second-order terms of the incremental quantities of Green-Lagrange normal strains in x and y directions, respectively, and they are given by

$$\hat{\varepsilon}_x^{(m)} = \left[\left(u_x^{(m)},_x \right)^2 + \left(u_y^{(m)},_x \right)^2 + \left(u_{\zeta}^{(m)},_x \right)^2 \right]/2 ,$$

$$\hat{\varepsilon}_y^{(m)} = \left[\left(u_x^{(m)},_y \right)^2 + \left(u_y^{(m)},_y \right)^2 + \left(u_\zeta^{(m)},_y \right)^2 \right] / 2 \ .$$

In this formulation, we take both the incremental displacement and the incremental transverse stress components to be the primary variables subject to variation. Using the kinematic and kinetic assumptions, given in Eqs. (6)-(11), we may express the first-order variation of the Reissner energy functional as follows

$$
\begin{aligned}
\delta \Pi_R = & \sum_{m=1}^{N_l} \int_{-h_m/2}^{h_m/2} \iint_\Omega \left\{ \left(\delta \boldsymbol{\varepsilon}_p^{(m)} \right)^T \boldsymbol{\sigma}_p^{(m)} + \left(\delta \boldsymbol{\varepsilon}_s^{(m)} \right)^T \boldsymbol{\sigma}_s^{(m)} + \delta \varepsilon_\zeta \, \sigma_\zeta^{(m)} + \left(\delta \boldsymbol{\sigma}_s^{(m)} \right)^T \right. \\
& \left(\boldsymbol{\varepsilon}_s^{(m)} - \mathbf{S}^{(m)} \boldsymbol{\sigma}_s^{(m)} \right) \\
& + \delta \sigma_\zeta^{(m)} \left[\varepsilon_\zeta^{(m)} - \left(c_{33}^{(m)} \right)^{-1} \sigma_\zeta^{(m)} + \left(\mathbf{Q}_\zeta^{(m)} \right)^T \boldsymbol{\varepsilon}_p^{(m)} \right] \bigg\} \, dx \, dy \, dz_m \\
& - \sum_{m=1}^{N_l} \int_{-h_m/2}^{h_m/2} \iint_\Omega \left(P_x \right) \left[\bar{f}_x^{(m)} \delta \hat{\varepsilon}_x^{(m)} + \bar{f}_y^{(m)} \delta \hat{\varepsilon}_y^{(m)} \right] dx \, dy \, dz_m \\
& - \sum_{m=1}^{N_l} \int_{-h_m/2}^{h_m/2} \int_{\Gamma_\sigma} \left(\bar{t}_k^{(m)} \, \delta u_k^{(m)} \right) d\Gamma \, dz_m - \int_{-h_m/2}^{h_m/2} \int_{\Gamma_u} \left(u_k^{(m)} - \bar{u}_k^{(m)} \right) \delta t_k^{(m)} \, d\Gamma \, dz_m
\end{aligned}
\tag{20}
$$

where the superscript T denotes the transposition of the matrices or vectors, and $k = x, y$ and ζ; and Γ_u and Γ_σ stand for the boundary edges, in which the essential and natural conditions are prescribed.

$$\boldsymbol{\varepsilon}_p^{(m)} = \begin{bmatrix} \varepsilon_x^{(m)} & \varepsilon_y^{(m)} & \gamma_{xy}^{(m)} \end{bmatrix}^T = \mathbf{B}_1^{(m)} \mathbf{u}^{(m)}, \qquad \boldsymbol{\varepsilon}_s^{(m)} = \begin{bmatrix} \gamma_{x\zeta}^{(m)} & \gamma_{y\zeta}^{(m)} \end{bmatrix}^T = \mathbf{B}_3^{(m)} \mathbf{u}^{(m)} + \mathbf{B}_4^{(m)} \mathbf{w}^{(m)}$$

$$\varepsilon_\zeta^{(m)} = \mathbf{B}_6^{(m)} \mathbf{w}^{(m)}, \qquad \boldsymbol{\sigma}_p^{(m)} = \begin{bmatrix} \sigma_x^{(m)} & \sigma_y^{(m)} & \tau_{xy}^{(m)} \end{bmatrix}^T = \mathbf{Q}_p^{(m)} \mathbf{B}_1^{(m)} \mathbf{u}^{(m)} + \mathbf{Q}_\zeta^{(m)} \mathbf{B}_2^{(m)} \boldsymbol{\sigma}^{(m)}$$

$$\boldsymbol{\sigma}_s^{(m)} = \begin{bmatrix} \tau_{x\zeta}^{(m)} & \tau_{y\zeta}^{(m)} \end{bmatrix}^T = \mathbf{B}_5^{(m)} \boldsymbol{\tau}^{(m)}, \qquad \sigma_\zeta^{(m)} = \mathbf{B}_2^{(m)} \boldsymbol{\sigma}^{(m)}$$

$$\hat{\varepsilon}_x^{(m)} = \frac{1}{2} \left(\mathbf{u}^{(m)} \right)^T \left(\mathbf{B}_7^{(m)} \right)^T \mathbf{B}_7^{(m)} \mathbf{u}^{(m)} + \frac{1}{2} \left(\mathbf{w}^{(m)} \right)^T \left(\mathbf{B}_8^{(m)} \right)^T \mathbf{B}_8^{(m)} \mathbf{w}^{(m)}$$

$$\hat{\varepsilon}_y^{(m)} = \frac{1}{2} \left(\mathbf{u}^{(m)} \right)^T \left(\mathbf{B}_9^{(m)} \right)^T \mathbf{B}_9^{(m)} \mathbf{u}^{(m)} + \frac{1}{2} \left(\mathbf{w}^{(m)} \right)^T \left(\mathbf{B}_{10}^{(m)} \right)^T \mathbf{B}_{10}^{(m)} \mathbf{w}^{(m)}$$

$$\mathbf{u}^{(m)} = \begin{bmatrix} u_i^{(m)} \\ v_i^{(m)} \end{bmatrix}_{i=1,2,\cdots,n_u+1}, \quad \mathbf{w}^{(m)} = \begin{bmatrix} w_i^{(m)} \end{bmatrix}_{i=1,2,\cdots,n_w+1}, \quad \boldsymbol{\tau}^{(m)} = \begin{bmatrix} \left(\tau_{13}^{(m)} \right)_i \\ \left(\tau_{23}^{(m)} \right)_i \end{bmatrix}_{i=1,2,\cdots,n_\tau+1} \quad \boldsymbol{\sigma}^{(m)} = \begin{bmatrix} \left(\sigma_3^{(m)} \right)_i \end{bmatrix}_{i=1,2,\cdots,n_\sigma+1},$$

$$\mathbf{S}^{(m)} = \begin{bmatrix} \left(1/c_{55}^{(m)} \right) & 0 \\ 0 & \left(1/c_{44}^{(m)} \right) \end{bmatrix}, \quad \mathbf{Q}_p^{(m)} = \begin{bmatrix} Q_{11}^{(m)} & Q_{12}^{(m)} & 0 \\ Q_{12}^{(m)} & Q_{22}^{(m)} & 0 \\ 0 & 0 & Q_{66}^{(m)} \end{bmatrix}, \quad \mathbf{Q}_\zeta^{(m)} = \begin{bmatrix} \left(c_{13}^{(m)} / c_{33}^{(m)} \right) \\ \left(c_{23}^{(m)} / c_{33}^{(m)} \right) \\ 0 \end{bmatrix}$$

and the detailed expressions of matrices $\mathbf{B}_k^{(m)}$ are given in Wu and Li (2010), and not repeated.

3.3. Euler−lagrange equations

The edge boundary conditions of each individual layer are considered as fully simple supports, which requires that the following quantities are satisfied.

$$u_y^{(m)} = u_\zeta^{(m)} = \sigma_x^{(m)} = 0 \qquad \text{at} \quad x = 0, \quad x = L_x \quad \text{and} \quad m = 1, 2, \cdots, N_l \tag{21a}$$

$$u_x^{(m)} = u_\zeta^{(m)} = \sigma_y^{(m)} = 0, \qquad \text{at} \quad y = 0, \quad y = L_y \quad \text{and} \quad m = 1, 2, \cdots, N_l \tag{21b}$$

By means of the separation of variables, the primary field variables of each individual layer are expanded as the following forms of a double Fourier series, so that the boundary conditions of the simply supported edges are exactly satisfied. They are given as

$$\left(u_x^{(m)}, \ \tau_{x\zeta}^{(m)} \right) = \sum_{\hat{m}=1}^{\infty} \sum_{\hat{n}=1}^{\infty} \left(u_{\hat{m}\hat{n}}^{(m)}, \ \tau_{13\hat{m}\hat{n}}^{(m)} \right) \cos \tilde{m} x \ \sin \tilde{n} y \tag{22}$$

$$\left(u_y^{(m)}, \ \tau_{y\zeta}^{(m)} \right) = \sum_{\hat{m}=1}^{\infty} \sum_{\hat{n}=1}^{\infty} \left(v_{\hat{m}\hat{n}}^{(m)}, \ \tau_{23\hat{m}\hat{n}}^{(m)} \right) \sin \tilde{m} x \ \cos \tilde{n} y \tag{23}$$

$$\left(u_\zeta^{(m)}, \ \sigma_\zeta^{(m)} \right) = \sum_{\hat{m}=1}^{\infty} \sum_{\hat{n}=1}^{\infty} \left(w_{\hat{m}\hat{n}}^{(m)}, \ \sigma_{3\hat{m}\hat{n}}^{(m)} \right) \sin \tilde{m} x \ \sin \tilde{n} y \tag{24}$$

in which $\tilde{m} = \hat{m} \pi / L_x$, $\tilde{n} = \hat{n} \pi / L_y$; and $\hat{m}$ and $\hat{n}$ are positive intergers.

Introducing Eqs. (22)-(24) in Eq. (20) and imposing the stationary principle of the Reissner energy functional (i.e., $\delta \Pi_R = 0$), we obtain the Euler−Lagrange equations of the plate as follows

$$\sum_{m=1}^{N_l} \left(\begin{bmatrix} \mathbf{K}_{\mathrm{I\ I}}^{(m)} & \mathbf{0} & \mathbf{K}_{\mathrm{I\ III}}^{(m)} & \mathbf{K}_{\mathrm{I\ IV}}^{(m)} \\ \mathbf{0} & \mathbf{0} & \mathbf{K}_{\mathrm{II\ III}}^{(m)} & \mathbf{K}_{\mathrm{II\ IV}}^{(m)} \\ \mathbf{K}_{\mathrm{III\ I}}^{(m)} & \mathbf{K}_{\mathrm{III\ II}}^{(m)} & \mathbf{K}_{\mathrm{III\ III}}^{(m)} & \mathbf{0} \\ \mathbf{K}_{\mathrm{IV\ I}}^{(m)} & \mathbf{K}_{\mathrm{IV\ II}}^{(m)} & \mathbf{0} & \mathbf{K}_{\mathrm{IV\ IV}}^{(m)} \end{bmatrix} - (P_x) \begin{bmatrix} \mathbf{G}_{\mathrm{I\ I}}^{(m)} & \mathbf{0} & \mathbf{0} & \mathbf{0} \\ \mathbf{0} & \mathbf{G}_{\mathrm{II\ II}}^{(m)} & \mathbf{0} & \mathbf{0} \\ \mathbf{0} & \mathbf{0} & \mathbf{0} & \mathbf{0} \\ \mathbf{0} & \mathbf{0} & \mathbf{0} & \mathbf{0} \end{bmatrix} \right) \begin{bmatrix} \tilde{\mathbf{u}}^{(m)} \\ \tilde{\mathbf{w}}^{(m)} \\ \tilde{\boldsymbol{\tau}}^{(m)} \\ \tilde{\boldsymbol{\sigma}}^{(m)} \end{bmatrix} = \begin{bmatrix} \mathbf{0} \\ \mathbf{0} \\ \mathbf{0} \\ \mathbf{0} \end{bmatrix} \tag{25}$$

where $\quad \mathbf{K}_{i\ j}^{(m)} = \left(\mathbf{K}_{j\ i}^{(m)} \right)^T \ (i, j = \mathbf{I, II, III, IV});\qquad \mathbf{K}_{\mathrm{I\ I}}^{(m)} = \int_{-h_m/2}^{h_m/2} \left(\tilde{\mathbf{B}}_1^{(m)} \right)^T \mathbf{Q}_p^{(m)} \tilde{\mathbf{B}}_1^{(m)} \ dz_m$,

$\mathbf{K}_{\mathrm{I\ III}}^{(m)} = \int_{-h_m/2}^{h_m/2} \left(\mathbf{B}_3^{(m)} \right)^T \mathbf{B}_5^{(m)} \ dz_m$, $\qquad \mathbf{K}_{\mathrm{I\ IV}}^{(m)} = \int_{-h_m/2}^{h_m/2} \left(\tilde{\mathbf{B}}_1^{(m)} \right)^T \mathbf{Q}_\zeta^{(m)} \mathbf{B}_2^{(m)} \ dz_m$,

$\mathbf{K}_{\mathrm{II\ III}}^{(m)} = \int_{-h_m/2}^{h_m/2} \left(\tilde{\mathbf{B}}_4^{(m)} \right)^T \mathbf{B}_5^{(m)} \ dz_m$, $\qquad \mathbf{K}_{\mathrm{II\ IV}}^{(m)} = \int_{-h_m/2}^{h_m/2} \left(\mathbf{B}_6^{(m)} \right)^T \mathbf{B}_2^{(m)} \ dz_m$,

$\mathbf{K}_{\mathrm{III\ III}}^{(m)} = -\int_{-h_m/2}^{h_m/2} \left(\mathbf{B}_5^{(m)} \right)^T \mathbf{S}^{(m)} \mathbf{B}_5^{(m)} \ dz_m$, $\qquad \mathbf{K}_{\mathrm{IV\ IV}}^{(m)} = -\int_{-h_m/2}^{h_m/2} \left(1/c_{33}^{(m)} \right) \left(\mathbf{B}_2^{(m)} \right)^T \mathbf{B}_2^{(m)} \ dz_m$;

$\mathbf{G}_{\mathrm{I\ I}}^{(m)} = \int_{-h_m/2}^{h_m/2} \left[\left(\tilde{\mathbf{B}}_7^{(m)} \right)^T \tilde{\mathbf{B}}_7^{(m)} \bar{f}_x^{(m)} + \left(\tilde{\mathbf{B}}_9^{(m)} \right)^T \tilde{\mathbf{B}}_9^{(m)} \bar{f}_y^{(m)} \right] dz_m$,

$\mathbf{G}_{\mathrm{II\ II}}^{(m)} = \int_{-h_m/2}^{h_m/2} \left[\left(\tilde{\mathbf{B}}_8^{(m)} \right)^T \tilde{\mathbf{B}}_8^{(m)} \bar{f}_x^{(m)} + \left(\tilde{\mathbf{B}}_{10}^{(m)} \right)^T \tilde{\mathbf{B}}_{10}^{(m)} \bar{f}_y^{(m)} \right] dz_m$;

$\tilde{\mathbf{u}}^{(m)} = \begin{bmatrix} \left(u_{\hat{m}\hat{n}}^{(m)} \right)_i \\ \left(v_{\hat{m}\hat{n}}^{(m)} \right)_i \end{bmatrix}_{i=1,2,\cdots,n_u+1}$, $\qquad \tilde{\mathbf{w}}^{(m)} = \left[\left(w_{\hat{m}\hat{n}}^{(m)} \right)_i \right]_{i=1,2,\cdots,n_w+1}$, $\qquad \tilde{\boldsymbol{\tau}}^{(m)} = \begin{bmatrix} \left(\tau_{13\hat{m}\hat{n}}^{(m)} \right)_l \\ \left(\tau_{23\hat{m}\hat{n}}^{(m)} \right)_l \end{bmatrix}_{i=1,2,\cdots,n_\tau+1}$,

$\tilde{\boldsymbol{\sigma}}^{(m)} = \left[\left(\sigma_{3\hat{m}\hat{n}}^{(m)} \right)_i \right]_{i=1,2,\cdots,n_\sigma+1}$;

the detailed expressions of matrices $\tilde{\mathbf{B}}_k^{(m)}$ are also given in the Appendix.

Using Eq. (25) and assembling the local linear and geometric stiffness matrices of each layer constituting the plate by following the standard process of the FEMs, in which the displacement and transverse stress continuity conditions at the interfaces between adjacent layers are imposed

and thus satisfied *a priori* for these RMVT-based FRLMs, we may construct the global linear and geometric stiffness matrices for the plate, which are given as

$$
\left(
\begin{bmatrix}
\mathbf{K}_{11} & \mathbf{0} & \mathbf{K}_{13} & \mathbf{K}_{14} \\
\mathbf{0} & \mathbf{0} & \mathbf{K}_{23} & \mathbf{K}_{24} \\
\mathbf{K}_{31} & \mathbf{K}_{32} & \mathbf{K}_{33} & \mathbf{0} \\
\mathbf{K}_{41} & \mathbf{K}_{42} & \mathbf{0} & \mathbf{K}_{44}
\end{bmatrix}
- (P_x)
\begin{bmatrix}
\mathbf{G}_{11} & \mathbf{0} & \mathbf{0} & \mathbf{0} \\
\mathbf{0} & \mathbf{G}_{22} & \mathbf{0} & \mathbf{0} \\
\mathbf{0} & \mathbf{0} & \mathbf{0} & \mathbf{0} \\
\mathbf{0} & \mathbf{0} & \mathbf{0} & \mathbf{0}
\end{bmatrix}
\right)
\begin{bmatrix}
\mathbf{u} \\
\mathbf{w} \\
\boldsymbol{\tau} \\
\boldsymbol{\sigma}
\end{bmatrix}
=
\begin{bmatrix}
\mathbf{0} \\
\mathbf{0} \\
\mathbf{0} \\
\mathbf{0}
\end{bmatrix}
\tag{26}
$$

Eq. (26) represents a standard eigenvalue problem, and a nontrivial solution of this exists if the determinant of the coefficient matrix vanishes. The critical loads, $(P_x)_{cr}$, of the plate for a set of fixed values $(\hat{m}, \hat{n})$ can be obtained by

$$
\left\|
\begin{bmatrix}
\mathbf{K}_{11} & \mathbf{0} & \mathbf{K}_{13} & \mathbf{K}_{14} \\
\mathbf{0} & \mathbf{0} & \mathbf{K}_{23} & \mathbf{K}_{24} \\
\mathbf{K}_{31} & \mathbf{K}_{32} & \mathbf{K}_{33} & \mathbf{0} \\
\mathbf{K}_{41} & \mathbf{K}_{42} & \mathbf{0} & \mathbf{K}_{44}
\end{bmatrix}
- (P_x)
\begin{bmatrix}
\mathbf{G}_{11} & \mathbf{0} & \mathbf{0} & \mathbf{0} \\
\mathbf{0} & \mathbf{G}_{22} & \mathbf{0} & \mathbf{0} \\
\mathbf{0} & \mathbf{0} & \mathbf{0} & \mathbf{0} \\
\mathbf{0} & \mathbf{0} & \mathbf{0} & \mathbf{0}
\end{bmatrix}
\right\|
= 0
\tag{27}
$$

Once Eq. (27) is solved, the eigenvalues and their corresponding eigenvectors, which are the critical loads and their corresponding modal field variables at each nodal plane, respectively, can be obtained.

4. Illustrative examples

In the following examples, $\mathrm{LM}_{n_u \ n_w}^{n_\tau \ n_\sigma}$ is defined to represent various RMVT-based FRLMs, in which the in- and out-of-plane displacements are expanded as the n_u- and n_w-order Lagrange polynomials, respectively, in the thickness coordinate of each layer, and the transverse shear and normal stresses are expanded as the n_τ- and n_σ-order ones. In addition, the implementation of various RMVT-based FRLMs for the bending analysis of multilayered FRCM/FGM plates (Wu and Li 2010) showed that letting $n_u = n_w = n_\tau = n_\sigma$ in the formulation will lead to efficient and stable computation, and it is therefore adopted for this work, in which the values of n_k ($k = u, v, \tau$ and σ) are taken as 1, 2, and 3 for the *h*-refinement process.

4.1 Laminated composite plates

Table 1 shows convergence studies for the present solutions of the lowest critical load parameters of $[0^0 / 90^0]_s$ plates under uni-axial compression (i.e., $k_p = 0$) and with different orthotropic ratios, in which the critical load parameter, and the material properties of each layer constituting the plates and their geometric parameters, are given as follows

$$
(\bar{P}_x)_{cr} = (P_x)_{cr} \, L_y / (E_T \, h^3) \quad \text{or} \quad (\bar{P}_x)_{cr} = (p_x)_{cr} \, L_y^2 / (E_T \, h^3)
\tag{28}
$$

$$
E_L / E_T = 3, 10, 20, 30 \text{ and } 40, \quad G_{LT} / E_T = 0.6, \quad G_{TT} / E_T = 0.5, \quad \upsilon_{LT} = \upsilon_{TT} = 0.25
\tag{29a-d}
$$

Table 1 Convergence studies for the present solutions of the lowest critical load parameters of laminated $[0^0 / 90^0]$ s plates under uni-axial compression and with different orthotropic ratios

Theories	E_L / E_T; $(\hat{m}, \hat{n})$				
	3; (1,1)	10; (1,1)	20; (1, 1)	30; (1, 1)	40; (1,1)
Present LM_{11}^{11} ($N_l = 4$)	5.3046 (5.3278)	9.7823 (9.8428)	15.0905 (15.1831)	19.4385 (19.5528)	23.0817 (23.2122)
Present LM_{11}^{11} ($N_l = 8$)	5.3017 (5.3248)	9.7598 (9.8196)	15.0180 (15.1088)	19.3044 (19.4162)	22.8829 (23.0101)
Present LM_{11}^{11} ($N_l = 16$)	5.3015 (5.3247)	9.7594 (9.8191)	15.0169 (15.1077)	19.3023 (19.4140)	22.8793 (23.0065)
Present LM_{11}^{11} ($N_l = 32$)	5.3015 (5.3246)	9.7594 (9.8191)	15.0168 (15.1076)	19.3021 (19.4139)	22.8790 (23.0062)
Present LM_{11}^{11} ($N_l = 40$)	5.3015 (5.3246)	9.7594 (9.8191)	15.0168 (15.1076)	19.3021 (19.4138)	22.8790 (23.0062)
Present LM_{22}^{22} ($N_l = 4$)	5.3017 (5.3248)	9.7600 (9.8197)	15.0185 (15.1093)	19.3053 (19.4170)	22.8840 (23.0112)
Present LM_{22}^{22} ($N_l = 8$)	5.3015 (5.3247)	9.7594 (9.8191)	15.0169 (15.1077)	19.3023 (19.4140)	22.8793 (23.0065)
Present LM_{22}^{22} ($N_l = 16$)	5.3015 (5.3246)	9.7594 (9.8191)	10.0167 (15.1076)	19.3021 (19.4139)	22.8790 (23.0062)
Present LM_{22}^{22} ($N_l = 32$)	5.3015 (5.3246)	9.7594 (9.8191)	10.0168 (15.1076)	19.3021 (19.4138)	22.8790 (23.0062)
Present LM_{22}^{22} ($N_l = 40$)	5.3015 (5.3246)	9.7594 (9.8191)	10.0167 (15.1076)	19.3021 (19.4138)	22.8790 (23.0062)
Present LM_{33}^{33} ($N_l = 4$)	5.3015 (5.3246)	9.7594 (9.8191)	15.0168 (15.1076)	19.3021 (19.4138)	22.8790 (23.0062)
Present LM_{33}^{33} ($N_l = 8$)	5.3015 (5.3246)	9.7594 (9.8191)	15.0168 (15.1076)	19.3021 (19.4138)	22.8790 (23.0062)
Present LM_{33}^{33} ($N_l = 16$)	5.3015 (5.3246)	9.7594 (9.8191)	15.0168 (15.1076)	19.3021 (19.4138)	22.8790 (23.0062)
Present LM_{33}^{33} ($N_l = 32$)	5.3015 (5.3246)	9.7594 (9.8191)	15.0168 (15.1076)	19.3021 (19.4138)	22.8790 (23.0062)
Present LM_{33}^{33} ($N_l = 40$)	5.3015 (5.3246)	9.7594 (9.8191)	15.0168 (15.1076)	19.3021 (19.4138)	22.8790 (23.0062)
Exact 3D solutions (Noor 1975)	5.3044	9.7621	15.0191	19.3040	22.8807
LM4 (D'Ottavio and Carrera 2010)	5.3051	9.7628	15.0196	19.3045	22.8811
LM2 (D'Ottavio and Carrera 2010)	5.3061	9.7673	15.0328	19.3301	22.9220
EMZ4 (D'Ottavio and Carrera 2010)	5.3056	9.7704	15.0485	19.3635	22.9761
EMZ3 (D'Ottavio and Carrera 2010)	5.3153	9.8147	15.1674	19.5679	23.2667

Table 1 Continued

Theories	E_L / E_T; $(\hat{m}, \hat{n})$				
	3; (1 ,1)	10; (1 ,1)	20; (1, 1)	30; (1, 1)	40; (1 ,1)
LD2 (D'Ottavio and Carrera 2010)	5.3066	9.7710	15.0423	19.3584	22.9690
EDZ4 (D'Ottavio and Carrera 2010)	5.3056	9.7710	15.0508	19.3684	22.9842
ED3 (D'Ottavio and Carrera 2010)	5.3060	9.7720	15.0551	19.3785	23.0021
ED2 (D'Ottavio and Carrera 2010)	5.3556	9.9945	15.6458	20.4027	24.4816
FSDT (D'Ottavio and Carrera 2010)	5.3991	9.9653	15.3513	19.7566	23.4529
CLPT (D'Ottavio and Carrera 2010)	5.7538	11.4918	19.7124	27.9357	36.1597

The solutions in parentheses are obtained using the uniform stress assumption for the pre-buckling state of stress.

$$L_x / L_y = 1, \quad L_x / h = 10 \tag{30a, b}$$

in which the subscripts, *L* and *T*, denote the directions parallel and transverse to the fiber directions, respectively.

It can be seen in Table 1 that the performances of various RMVT-based FRLMs are $\text{LM}_{33}^{33} > \text{LM}_{22}^{22} > \text{LM}_{11}^{11}$, in which ">" means better accuracy and faster convergence rate. The convergent solutions are obtained at $N_l = 32$, 16 and 4 for LM_{11}^{11}, LM_{22}^{22} and LM_{33}^{33}, respectively, when $E_L / E_T = 40$, while at $N_l = 16$, 8 and 4 when $E_L / E_T = 3$, which means the convergence rates of various FRLMs increase as the orthotropic ratio becomes smaller. The solutions in parentheses are obtained using the uniform stress assumption for the pre-buckling state of stress, in which the influence functions $\bar{f}_x^{(m)}$ and $\bar{f}_y^{(m)}$ based on the constant strain assumption, which are given in Eqs. (5(a) and 5(b)), are simply replaced by $\bar{f}_x^{(m)} = 1/(L_y \, h)$ and $\bar{f}_y^{(m)} = 0$. It is shown that higher critical load parameters are obtained when the constant stress assumption is used, and the deviations between these solutions on the basis of the constant strain and stress assumptions increase when the orthotropic ratio becomes larger although these are minor, which are less than 0.6% in these cases.

The present RMVT-based FRLM solutions are also compared with the exact 3D ones (Noor 1975) and those from some of classical and more advanced 2D theories available in the literature (D'Ottavio and Carrera 2010), such as the RMVT-based second- and fourth-order layerwise theories (i.e., LM2 and LM4), PVD-based second-order layerwise theory (i.e., LD2), PVD-based ESLTs with first-, second- and third-order models (i.e., FSDT, ED2 and ED3), PVD-based ESLT with fourth-order model accounting for the zig-zag effect (i.e., EDZ4), RMVT-based ESLT with third- and fourth-order models accounting for the zig-zag effect (i.e., EMZ3 and EMZ4), and

classical lamination plate theory (CLPT). It can be seen in Table 1 that the present convergent solutions are in excellent agreement with the exact 3D and accurate 2D ones obtained using LM4, and ESLTs may provide the accurate solutions for the plates with low orthotropic ratios, whereas layerwise theories are required for the plates with high orthotropic ratios.

Table 2 shows convergence studies for the present solutions of the lowest critical load parameters of $[0^0 / 90^0]_s$ plates under uni- and bi-axial compression (i.e., $k_p = 0$ and $k_p \neq 0$, respectively) and with different length-to-thickness ratios, in which the load intensity ratio, the material properties of each layer constituting the plates, and their geometric parameters are given as follows

$$k_p = 0, 0.25, 0.5, 0.75, 1.0 \tag{31}$$

$$E_L / E_T = 25, \quad G_{LT} / E_T = 0.6, \quad G_{TT} / E_T = 0.5, \quad \upsilon_{LT} = \upsilon_{TT} = 0.25 \tag{32a-d}$$

$$L_x / L_y = 1, \quad L_x / h = 10, 50 \tag{33a, b}$$

It can be seen in Table 2 that the convergent solutions are obtained at $N_l = 32$, 16 and 4 for LM_{11}^{11}, LM_{22}^{22} and LM_{33}^{33}, respectively, when $L_x / h = 10$, while at $N_l = 8$, 4 and 4 when $L_x / h = 50$, which means the convergence rates of various FRLMs increase as the plate becomes thinner. The solutions in parentheses are obtained using von K′arm′an′s approximation, in which the second-order terms of the incremental quantities of Green-Lagrange normal strains in x and y directions, which are given in Eq. (19), are simply approximated by $\hat{\varepsilon}_x^{(m)} = \left(u_\zeta^{(m)},_x \right)^2 / 2$ and $\hat{\varepsilon}_y^{(m)} = \left(u_\zeta^{(m)},_y \right)^2 / 2$. Higher critical load parameters are obtained when von K′arm′an′s approximation is used, and the deviations between these solutions on the basis of the full kinematic nonlinearity and the von K′arm′an′s approximation increase when the plate becomes thicker, and are about 2% for the moderately thick plates ($L_x / h = 10$) and less than 0.2% for the thin ones ($L_x / h = 50$).

Table 2 Convergence studies for the present solutions of the lowest critical load parameters of laminated $[0^0 / 90^0]_s$ plates under uni- and bi-axial compression and with different total number of layers and load intensity ratios

L_x / h	Theories	$k_p; (\hat{m}, \hat{n})$				
		0; (1, 1)	0.25;(1, 1)	0.5; (1, 1)	0.75; (1, 1)	1; (1, 1)
10	Present LM_{11}^{11} ($N_l = 4$)	17.3661 (17.6943)	13.9271 (14.1455)	11.6245 (11.7818)	9.9749 (10.0947)	8.7352 (8.8301)
	Present LM_{11}^{11} ($N_l = 8$)	17.2636 (17.5890)	13.8445 (14.0612)	11.5552 (11.7115)	9.9153 (10.0344)	8.6829 (8.7773)
	Present LM_{11}^{11} ($N_l = 16$)	17.2620 (17.5873)	13.8432 (14.0598)	11.5541 (11.7103)	9.9143 (10.0334)	8.6821 (8.7764)
	Present LM_{11}^{11} ($N_l = 32$)	17.2619 (17.5872)	13.8431 (14.0597)	11.5540 (11.7103)	9.9143 (10.0333)	8.6820 (8.7764)

Table 2 Continued

L_x/h	Theories	k_p; $(\hat{m}, \hat{n})$				
		0; (1, 1)	0.25;(1, 1)	0.5; (1, 1)	0.75; (1, 1)	1; (1, 1)
	Present LM_{11}^{11} ($N_l = 40$)	17.2619 (17.5872)	13.8431 (14.0597)	11.5540 (11.7103)	9.9143 (10.0333)	8.6820 (8.7764)
	Present LM_{22}^{22} ($N_l = 4$)	17.2643 (17.5897)	13.8450 (14.0617)	11.5556 (11.7119)	9.9157 (10.0347)	8.6832 (8.7776)
	Present LM_{22}^{22} ($N_l = 8$)	17.2620 (17.5873)	13.8432 (14.0599)	11.5541 (11.7104)	9.9144 (10.0334)	8.6821 (8.7764)
	Present LM_{22}^{22} ($N_l = 16$)	17.2619 (17.5872)	13.8431 (14.0597)	11.5540 (11.7103)	9.9143 (10.0333)	8.6820 (8.7764)
	Present LM_{22}^{22} ($N_l = 32$)	17.2619 (17.5872)	13.8431 (14.0597)	11.5540 (11.7103)	9.9143 (10.0333)	8.6820 (8.7764)
	Present LM_{22}^{22} ($N_l = 40$)	17.2619 (17.5872)	13.8431 (14.0597)	11.5540 (11.7103)	9.9143 (10.0333)	8.6820 (8.7764)
	Present LM_{33}^{33} ($N_l = 4$)	17.2619 (17.5872)	13.8431 (14.0597)	11.5540 (11.7103)	9.9143 (10.0333)	8.6820 (8.7764)
	Present LM_{33}^{33} ($N_l = 8$)	17.2619 (17.5872)	13.8431 (14.0597)	11.5540 (11.7103)	9.9143 (10.0333)	8.6820 (8.7764)
	Present LM_{33}^{33} ($N_l = 16$)	17.2619 (17.5872)	13.8431 (14.0597)	11.5540 (11.7103)	9.9143 (10.0333)	8.6820 (8.7764)
	Present LM_{33}^{33} ($N_l = 32$)	17.2619 (17.5872)	13.8431 (14.0597)	11.5540 (11.7103)	9.9143 (10.0333)	8.6820 (8.7764)
	Present LM_{33}^{33} ($N_l = 40$)	17.2619 (17.5872)	13.8431 (14.0597)	11.5540 (11.7103)	9.9143 (10.0333)	8.6820 (8.7764)
	LM4 (D'Ottavio and Carrera 2010)	17.2645	NA	NA	NA	8.6820
	LM2 (D'Ottavio and Carrera 2010)	17.2835	NA	NA	NA	8.6914
	EMZ4 (D'Ottavio and Carrera 2010)	17.3075	NA	NA	NA	8.7010
	EM3 (D'Ottavio and Carrera 2010)	17.3145	NA	NA	NA	8.7043
	EDZ4 (D'Ottavio and Carrera 2010)	17.3110	NA	NA	NA	8.7028
	ED4 (D'Ottavio and Carrera 2010)	17.3127	NA	NA	NA	8.7057
	FSDT (D'Ottavio and Carrera 2010)	17.6568	NA	NA	NA	8.8284
	CLT (D'Ottavio and Carrera 2010)	23.8239	NA	NA	NA	11.9120
50	Present LM_{11}^{11} ($N_l = 4$)	23.4645 (23.4903)	18.7740 (18.7913)	15.6464 (15.6589)	13.4120 (13.4215)	11.7361 (11.7436)

Table 2 Continued

L_x / h	Theories	k_p; $(\hat{m}, \hat{n})$				
		0; (1, 1)	0.25;(1, 1)	0.5; (1, 1)	0.75; (1, 1)	1; (1, 1)
	Present LM$_{11}^{11}$ ($N_l = 8$)	23.4563 (23.4821)	18.7675 (18.7847)	15.6410 (15.6534)	13.4074 (13.4169)	11.7320 (11.7396)
	Present LM$_{11}^{11}$ ($N_l = 16$)	23.4563 (23.4821)	18.7675 (18.7847)	15.6409 (15.6534)	13.4073 (13.4168)	11.7320 (11.7395)
	Present LM$_{11}^{11}$ ($N_l = 32$)	23.4563 (23.4821)	18.7675 (18.7847)	15.6409 (15.6534)	13.4073 (13.4168)	11.7320 (11.7395)
	Present LM$_{11}^{11}$ ($N_l = 40$)	23.4563 (23.4821)	18.7675 (18.7847)	15.6409 (15.6534)	13.4073 (13.4168)	11.7320 (11.7395)
	Present LM$_{22}^{22}$ ($N_l = 4$)	23.4564 (23.4822)	18.7676 (18.7848)	15.6410 (15.6535)	13.4074 (13.4169)	11.7320 (11.7396)
	Present LM$_{22}^{22}$ ($N_l = 8$)	23.4563 (23.4821)	18.7675 (18.7847)	15.6409 (15.6534)	13.4073 (13.4168)	11.7320 (11.7395)
	Present LM$_{22}^{22}$ ($N_l = 16$)	23.4563 (23.4821)	18.7675 (18.7847)	15.6409 (15.6534)	13.4073 (13.4168)	11.7320 (11.7395)
	Present LM$_{22}^{22}$ ($N_l = 32$)	23.4563 (23.4821)	18.7675 (18.7847)	15.6409 (15.6534)	13.4073 (13.4168)	11.7320 (11.7395)
	Present LM$_{22}^{22}$ ($N_l = 40$)	23.4563 (23.4821)	18.7675 (18.7847)	15.6409 (15.6534)	13.4073 (13.4168)	11.7320 (11.7395)
	Present LM$_{33}^{33}$ ($N_l = 4$)	23.4563 (23.4821)	18.7675 (18.7847)	15.6409 (15.6534)	13.4073 (13.4168)	11.7320 (11.7395)
	Present LM$_{33}^{33}$ ($N_l = 8$)	23.4563 (23.4821)	18.7675 (18.7847)	15.6409 (15.6534)	13.4073 (13.4168)	11.7320 (11.7395)
	Present LM$_{33}^{33}$ ($N_l = 16$)	23.4563 (23.4821)	18.7675 (18.7847)	15.6409 (15.6534)	13.4073 (13.4168)	11.7320 (11.7395)
	Present LM$_{33}^{33}$ ($N_l = 32$)	23.4563 (23.4821)	18.7675 (18.7847)	15.6409 (15.6534)	13.4073 (13.4168)	11.7320 (11.7395)
	Present LM$_{33}^{33}$ ($N_l = 40$)	23.4563 (23.4821)	18.7675 (18.7847)	15.6409 (15.6534)	13.4073 (13.4168)	11.7320 (11.7395)
	LM4 (D'Ottavio and Carrera 2010)	23.4565	NA	NA	NA	11.7320
	LM2 (D'Ottavio and Carrera 2010)	23.4575	NA	NA	NA	11.7325
	EMZ4 (D'Ottavio and Carrera 2010)	23.4588	NA	NA	NA	11.7331
	EM3 (D'Ottavio and Carrera 2010)	23.4591	NA	NA	NA	11.7333
	EDZ4 (D'Ottavio and Carrera 2010)	23.4590	NA	NA	NA	11.7332
	ED4 (D'Ottavio and Carrera 2010)	23.5693	NA	NA	NA	11.7334

Table 2 Continued

L_x / h	Theories	$k_p; (\hat{m}, \hat{n})$				
		0; (1, 1)	0.25;(1, 1)	0.5; (1, 1)	0.75; (1, 1)	1; (1, 1)
	FSDT (D'Ottavio and Carrera 2010)	23.4588	NA	NA	NA	11.7428
	CLT (D'Ottavio and Carrera 2010)	23.8239	NA	NA	NA	11.9120

The solutions in parentheses are obtained using von k′arm′an's approximation

Fig. 2 shows the variations of the present convergent solutions of the lowest critical load parameters with the length-to-width ratio for the $\left[0^0 / 90^0\right]_s$ plates under uni- and bi-axial compression (i.e., k_p=0, and k_p=0.5 and 1.0, respectively) and with $\hat{m}=1-5$, in which E_L / E_T =30, and other material properties are the same as those given in Eqs. (32(b)-32(d)); L_x / h=10 and L_x / L_y=0.5-10. Referring to the figures, the magnitude of the lowest critical load parameter and its corresponding number of half-waves ($\hat{m}$) for a wide range of the length-to-width ratio are shown using a solid dark line. It is observed in Fig. 2 that the lowest critical load parameter decreases as the load intensity ratio increases. In the cases of uni-axial compression ($k_p = 0$), the
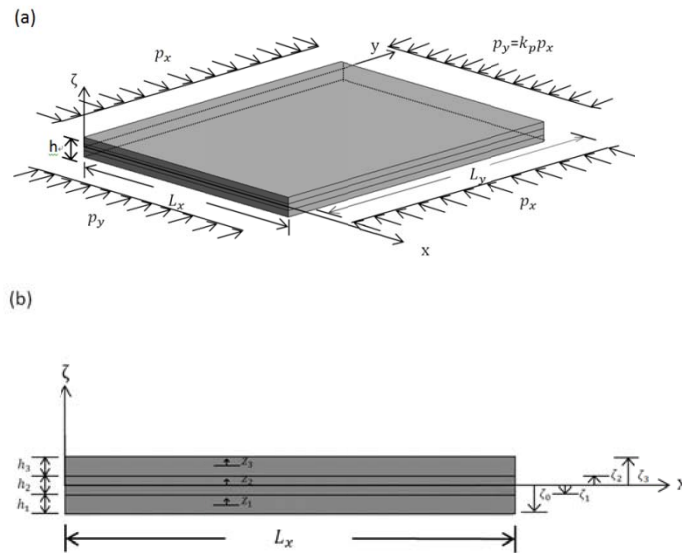

Fig. 1 (a) The configuration and loading conditions of a multilayered plate. (b) The global and local coordinates of the plate

lowest critical load parameter occurs at the first longitudinal mode ($\hat{m}$ =1) when the length-to-width ratio is low, about less than 2, and the dominant longitudinal mode will change in the series of 1- to 5 when this ratio increases from 0.5 to 10, while in the cases of bi-axial compression (k_p =0.5 and 1.0), the dominant longitudinal mode always occurs at the first longitudinal mode ($\hat{m}$ =1) when the length-to-width ratio increases from 0.5 to 10.

4.2 FGM sandwich plates

We consider the buckling responses of a simply-supported and uni- and bi-axially loaded, FGM sandwich plate consisting of a soft FGM core layer bounded with two stiff homogeneous face sheets, in which the thickness ratio for each layer of the sandwich plate is $h_1 : h_2 : h_3$, in which $h_1 = h_3$ and $\sum_{m=1}^{3} h_m = h$, as well as the effective engineering constants of each layer are written as follows

$$E^{(m)}(\zeta) = E_0 + (E_f - E_0)\Gamma^{(m)}(\zeta) \qquad (m\text{=1, 2 and 3}) \qquad (34a)$$

$$\upsilon^{(m)} = \text{constant} \qquad (m\text{=1, 2 and 3}) \qquad (34b)$$

in which E_0 denotes the Young's modulus of the material at the mid-surface of the core, for which E_0 =70 GPa (aluminum) and E_f =380 GPa (alumina) are used in this example; $\upsilon^{(m)}$ (*m*=1-3) are taken to be 0.3; $\Gamma^{(m)}$ (*m*=1-3) are the volume fractions of the constituents of the plate, and are given by

$$\Gamma^{(1)} = 1 \qquad \text{when } (-h/2) \le \zeta \le (-h_2/2) \qquad (35a)$$

$$\Gamma^{(2)}(\zeta) = \left[|\zeta|/(h_2/2) \right]^\kappa \qquad \text{when } (-h_2/2) \le \zeta \le (h_2/2) \qquad (35b)$$

$$\Gamma^{(3)} = 1 \qquad \text{when } (h_2/2) \le \zeta \le (h/2) \qquad (35c)$$

According to Eqs. (35(a)-35(c)), when κ =0, $\Gamma^{(2)} = 1$, this FGM sandwich plate reduces to a single-layered homogeneous plate with material properties E_f =380 GPa and υ_f =0.3; while when $\kappa = \infty$, $\Gamma^{(2)} = 0$, this FGM sandwich plate reduces to a homogeneous sandwich one with material properties $E^{(1)} = E^{(3)}$ =380 GPa, $E^{(2)}$ =70 GPa, and $\upsilon^{(m)}$ =0.3 (*m*=1-3). The critical load parameter in these FGM sandwich plate cases is defined as follows

$$\left(\overline{P}_x\right)_{cr} = \left(P_x\right)_{cr} L_y /\left(E_f h^3\right) \quad \text{or} \quad \left(\overline{P}_x\right)_{cr} = \left(p_x\right)_{cr} L_y^2 /\left(E_f h^3\right) \qquad (36)$$
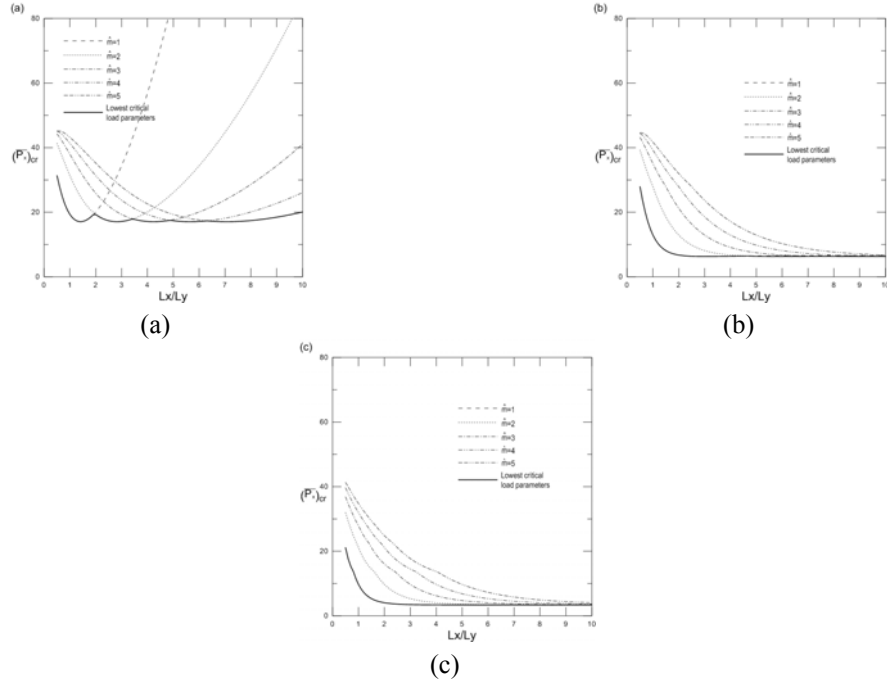
Fig. 2 Variations of the critical load parameters of uni- and bi-axially loaded, $\left[0^0 / 90^0\right]_S$ laminated plates with the length-to-width ratio for $\hat{m}$ =1-5, (a) $k_p = 0$, (b) $k_p = 0.5$, (c) $k_p = 1.0$

Table 3 shows the convergence studies of the present LM_{22}^{22} and LM_{33}^{33} solutions of the lowest critical load parameters of FGM sandwich plates under uni- and bi-axial compression, in which k_p =0.0, 0.5 and 1.0; N_l =10, 20, 40 and 80; $L_x = L_y$ and $L_x / h = 10$; $\kappa = 0$, 1, 5, 10 and ∞; $h_1 : h_2 : h_3 = 0.1h : 0.8h : 0.1h$. It can be seen in Table 3 that the convergence rate of these solutions of single-layered homogeneous plates ($\kappa = 0$) and homogeneous sandwich ones ($\kappa = \infty$) is faster than that of FGM sandwich plates, and the relative errors of the 20-layer $LM_{22}^{22} / LM_{33}^{33}$ solutions in comparison with the convergent solutions are about less than 0.3%. The critical load parameter for the FGM sandwich plate becomes smaller as the material-property gradient index (κ) increases, which means the global stiffness of the plate becomes softer. Table 4 shows the convergent LM_{22}^{22} and LM_{33}^{33} solutions of the lowest critical load parameters of FGM sandwich plates under uni- and bi-axial compression and with different load intensity ratios, thickness ratios for each layer, and material-property gradient indices, in which k_p =0.0, 0.5 and 1.0; N_l =80; $L_x = L_y$ and $L_x / h = 10$; $\kappa = 0$, 1, 5, 10 and ∞; $h_1 : h_2 : h_3 = 0.1h : 0.8h : 0.1h$, 0.2h:0.6h:0.2h and (h/3):(h/3): (h/3). It is shown that the lowest critical load parameter decreases when the load intensity ratio becomes larger, and this increases when the thickness of FGM layer becomes thinner. In addition, the lowest critical load occurs at the buckling modes with $\hat{m} = \hat{n} = 1$ for the moderately thick plates, in which $L_x / h = 10$.
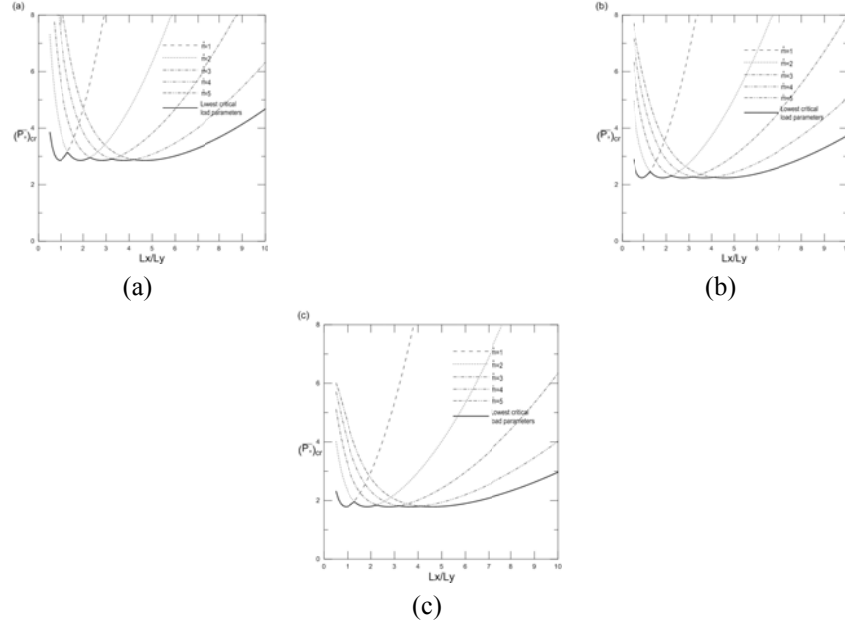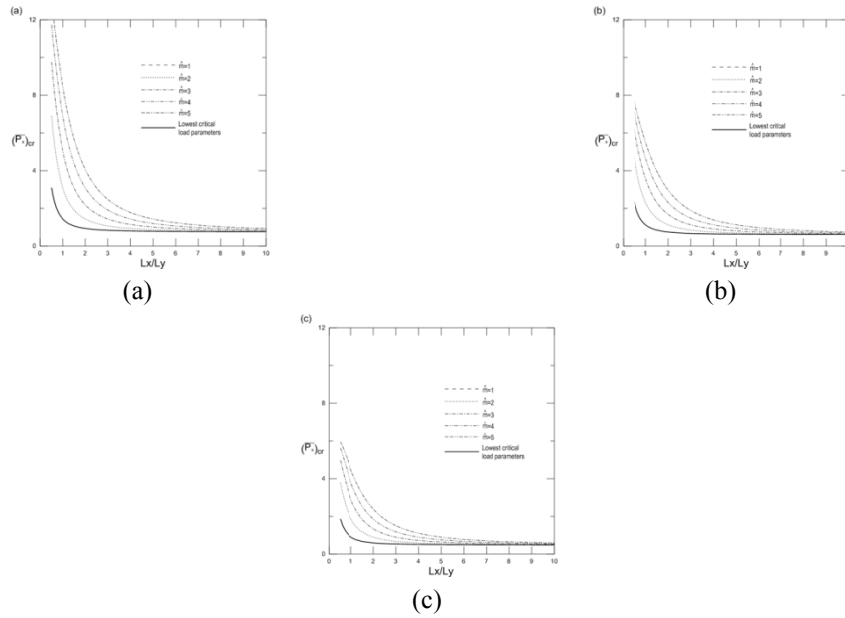
(a)

(b)

(c)

Fig. 3 Variations of the critical load parameters of uni-axially loaded, FGM sandwich plates with the length-to-width ratio for $\hat{m}$ =1-5 ($k_p = 0$), (a) $\kappa = 1$, (b) $\kappa = 5$, (c) $\kappa = \infty$

(a)

(b)

(c)

Fig. 4 Variations of the critical load parameters of bi-axially loaded, FGM sandwich plates with the length-to-width ratio for $\hat{m}$ =1-5 and $k_p = 1.0$, (a) $\kappa = 1$, (b) $\kappa = 5$, (c) $\kappa = \infty$.

Table 3 Convergence studies for the present solutions of the critical load parameters of FGM sandwich plates under uni- and bi-axial compressive loads and with different load intensity ratios and material-property gradient indices

k_p; $(\hat{m}, \hat{n})$	Theories	κ				
		0	1	5	10	∞
0.0; (1, 1)	Present LM_{22}^{22} (N_l=10)	3.3814	2.8605	2.2385	2.0528	1.7964
	Present LM_{22}^{22} (N_l=20)	3.3814	2.8681	2.2559	2.0685	1.7964
	Present LM_{22}^{22} (N_l=40)	3.3814	2.8698	2.2605	2.0732	1.7964
	Present LM_{22}^{22} (N_l= 80)	3.3814	2.8702	2.2616	2.0745	1.7964
	Present LM_{33}^{33} (N_l=10)	3.3814	2.8605	2.2385	2.0528	1.7964
	Present LM_{33}^{33} (N_l=20)	3.3814	2.8681	2.2559	2.0685	1.7964
	Present LM_{33}^{33} (N_l=40)	3.3814	2.8698	2.2605	2.0732	1.7964
	Present LM_{33}^{33} (N_l=80)	3.3814	2.8702	2.2616	2.0745	1.7964
0.5; (1, 1)	Present LM_{22}^{22} (N_l=10)	2.2542	1.9070	1.4923	1.3685	1.1976
	Present LM_{22}^{22} (N_l=20)	2.2542	1.9121	1.5039	1.3790	1.1976
	Present LM_{22}^{22} (N_l=40)	2.2542	1.9132	1.5070	1.3821	1.1976
	Present LM_{22}^{22} (N_l=80)	2.2542	1.9134	1.5078	1.3830	1.1976
	Present LM_{33}^{33} (N_l=10)	2.2542	1.9070	1.4923	1.3685	1.1976
	Present LM_{33}^{33} (N_l=20)	2.2542	1.9121	1.5039	1.3790	1.1976
	Present LM_{33}^{33} (N_l=40)	2.2542	1.9132	1.5070	1.3821	1.1976
	Present LM_{33}^{33} (N_l=80)	2.2542	1.9134	1.5078	1.3830	1.1976
1.0; (1, 1)	Present LM_{22}^{22} (N_l=10)	1.6907	1.4303	1.1192	1.0264	0.8982
	Present LM_{22}^{22} (N_l=20)	1.6907	1.4341	1.1279	1.0342	0.8982
	Present LM_{22}^{22} (N_l=40)	1.6907	1.4349	1.1302	1.0366	0.8982
	Present LM_{22}^{22} (N_l=80)	1.6907	1.4351	1.1308	1.0372	0.8982
	Present LM_{33}^{33} (N_l=10)	1.6907	1.4303	1.1192	1.0264	0.8982
	Present LM_{33}^{33} (N_l=20)	1.6907	1.4341	1.1279	1.0342	0.8982
	Present LM_{33}^{33} (N_l=40)	1.6907	1.4349	1.1302	1.0366	0.8982
	Present LM_{33}^{33} (N_l=80)	1.6907	1.4351	1.1308	1.0372	0.8982

Figs. 3 and 4 show the variations of the present convergent solutions of the critical load parameters of FGM sandwich plates with the length-to-width ratio, and under uni-axial (k_p=0) and bi-axial (k_p=1) compression, respectively, for $\hat{m}=1-5$, in which L_x/h=10, $h_1:h_2:h_3 = 0.1h:0.8h:0.1h$, κ=1, 5 and ∞. Referring to the figures, the magnitude of the lowest

critical load parameter and its corresponding number of half-waves ($\hat{m}$) for a wide range of the length-to-thickness ratio are shown using a solid dark line. It can be seen in Figs. 3 and 4 that the lowest critical load parameter decreases as the material-property gradient index becomes greater, which also means that the gross stiffness of the plate becomes decreases. Again, results of Fig. 3 shows that in the cases of uni-axial compression, the dominant longitudinal mode will change in the series of 1- to 5 when this ratio increases from 0.5 to 10; while those of Fig. 4 shows that in the cases of bi-axial compression, the dominant longitudinal mode always occurs at the first longitudinal mode ($\hat{m}$ =1) when the length-to-width ratio increases from 0.5 to 10.

Table 4 The present convergent solutions of the lowest critical load parameters of FGM sandwich plates under uni- and bi-axial compressive loads

k_p	$h_1 : h_2 : h_3$	$(\hat{m},\ \hat{n})$	Theories		κ			
				0	1	5	10	∞
0.0	$0.1h : 0.8h : 0.1h$	(1, 1)	Present LM$_{22}^{22}$	3.3814	2.8702	2.2616	2.0745	1.7964
			Present LM$_{33}^{33}$	3.3814	2.8702	2.2616	2.0745	1.7964
0.0	$0.2h : 0.6h : 0.2h$	(1, 1)	Present LM$_{22}^{22}$	3.3814	3.0779	2.6968	2.5891	2.4430
			Present LM$_{33}^{33}$	3.3814	3.0779	2.6968	2.5891	2.4430
0.0	$(h/3):(h/3):(h/3)$	(1, 1)	Present LM$_{22}^{22}$	3.3814	3.2489	3.0536	2.9993	2.9286
			Present LM$_{33}^{33}$	3.3814	3.2489	3.0536	2.9993	2.9286
0.5	$0.1h : 0.8h : 0.1h$	(1, 1)	Present LM$_{22}^{22}$	2.2542	1.9134	1.5078	1.3830	1.1976
			Present LM$_{33}^{33}$	2.2542	1.9134	1.5078	1.3830	1.1976
0.5	$0.2h : 0.6h : 0.2h$	(1, 1)	Present LM$_{22}^{22}$	2.2542	2.0519	1.7979	1.7261	1.6287
			Present LM$_{33}^{33}$	2.2542	2.0519	1.7979	1.7261	1.6287
0.5	$(h/3):(h/3):(h/3)$	(1, 1)	Present LM$_{22}^{22}$	2.2542	2.1659	2.0357	1.9995	1.9524
			Present LM$_{33}^{33}$	2.2542	2.1659	2.0357	1.9995	1.9524
1.0	$0.1h : 0.8h : 0.1h$	(1, 1)	Present LM$_{22}^{22}$	1.6907	1.4351	1.1308	1.0372	0.8982
			Present LM$_{33}^{33}$	1.6907	1.4351	1.1308	1.0372	0.8982
1.0	$0.2h : 0.6h : 0.2h$	(1, 1)	Present LM$_{22}^{22}$	1.6907	1.5389	1.3484	1.2946	1.2215
			Present LM$_{33}^{33}$	1.6907	1.5389	1.3484	1.2946	1.2215
1.0	$(h/3):(h/3):(h/3)$	(1, 1)	Present LM$_{22}^{22}$	1.6907	1.6245	1.5268	1.4996	1.4643
			Present LM$_{33}^{33}$	1.6907	1.6245	1.5268	1.4996	1.4643

Fig. 5 shows the variations of the present convergent solutions of the critical load parameters of FGM sandwich plates with the length-to-thickness ratio, and under bi-axial compression, in which $L_x = L_y$, $h_1 : h_2 : h_3 = 0.1h : 0.8h : 0.1h$, κ =1, 5 and ∞, and k_p =1. It is observed that the lowest critical load, rather than its parameter, decreases as the plate becomes narrower and thinner,

and that again the lowest critical load parameter occurs at the first longitudinal mode ($\hat{m}$ =1) for a wide range of the length-to-thickness ratios, which are L_x / h =1-1000, in these bi-axial compression cases. In addition, the variation patterns of the critical load parameters with different length-to-width and length-to-thickness ratios remain identical to those obtained using different material-property gradient indices, which means the critical buckling mode will not be affected by changing these.
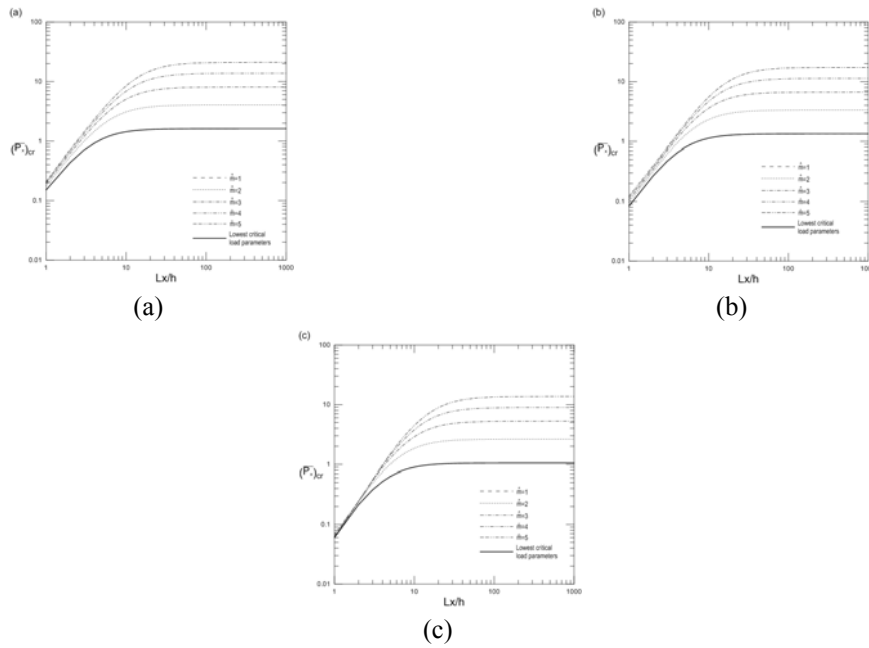

(a)   (b)

(c)

Fig. 5 Variations of the critical load parameters of bi-axially loaded, FGM sandwich plates with the length-to-thickness ratio for $\hat{m}$ =1-5 and $k_p = 1.0$, (a) $\kappa = 1$, (b) $\kappa = 5$, (c) $\kappa = \infty$

5. Conclusions

In this work, we developed a unified formulation of various RMVT-based FRLMs to investigate the buckling responses of simply-supported, multilayered composite plates and FGM sandwich ones under uni- and bi-axial compression. In the implementations of these methods with the *h*-refinement process, we find that the present solutions of the critical load parameters of LM_{22}^{22} and LM_{33}^{33} converge rapidly, and their convergent solutions are in excellent agreement with the exact 3D and accurate 2D ones available in the literature. It is shown in the illustrative examples that higher critical loads are obtained when the pre-buckling state of stress is determined on the basis of the constant stress assumption, rather than the constant strain one, although the deviation between these two solutions is minor. Higher critical loads are also obtained when von K$'$arm$'$an$'$s approximation, rather than full kinematic nonlinearity, is used, and the deviation between these two solutions is negligible in practic for the thin-plate case, while it increases as the plate becomes thicker. The lowest critical load decreases as the load intensity ratio and the

material-property gradient index increases, and also as the plate becomes narrower and thinner. In addition, changing the material-property gradient index will not affect the dominant buckling mode.

Acknowledgments

References

Akhras, G. and Li, W.C. (2007), "Three-dimensional static, vibration and stability analysis of piezoelectric composite plates using a finite layer method", *Smart Mater. Struct.*, **16**(3), 561-569.

Akhras, G. and Li, W.C. (2008), "Three-dimensional thermal buckling analysis of piezoelectric composite plates using the finite layer method", *Smart Mater. Struct.*, **17**(5), 1-8.

Brischetto, S. and Carrera, E. (2010), "Advanced mixed theories for bending analysis of functionally graded plates", *Comput. Struct.*, **88**(23-24), 1474-1483.

Carrera, E. (2000a), "A priori vs. a posteriori evaluation of transverse stresses in multilayered orthotropic plates", *Compos. Struct.*, **48**(4), 245-260.

Carrera, E. (2000b), "An assessment of mixed and classical theories on global and local response of multilayered orthotropic plates", *Compos. Struct.*, **50**(2), 183-198.

Carrera E. (2001), "Developments, ideas, and evaluations based upon Reissner's Mixed Variational Theorem in the modeling of multilayered plates and shells", *Appl. Mech. Rev.*, **54**, 301-329.

Carrera, E. (2003a), "Historical review of zig-zag theories for multilayered plates and shells", *Appl. Mech. Rev.*, **56**, 287-308.

Carrera, E. (2003b), "Theories and finite elements for multilayered plates and shells: A unified compact formulation with numerical assessment and benchmarks", *Arch. Comput. Method. E.*, **10**(3), 215-296.

Carrera, E. and Brischetto, S. (2009), "A survey with numerical assessment of classical and refined theories for the analysis of sandwich plates", *Appl. Mech. Rev.*, **62**, 1-17.

Carrera, E., Brischetto, S., Cinefra, M. and Soave, M. (2010), "Refined and advanced models for multilayered plates and shells embedding functionally graded material layers", *Mech. Adv. Mater. Struct.*, **17**(8), 603-621.

Carrera, E., Brischetto, S. and Robaldo, A. (2008), "A variable kinematic model for the analysis of functionally graded material plates", *AIAA J.*, **46**(1), 194-203.

Carrera, E. and Ciuffreda, A. (2005a), "Bending of composites and sandwich plates subjected to localized lateral loadings: A comparison of various theories", *Compos. Struct.*, **68**(2), 185-202.

Carrera, E. and Ciuffreda, A. (2005b), "A unified formulation to assess theories of multilayered plates for various bending problems", *Compos. Struct.*, **69**(3), 271-293.

Cheung, Y.K., Jiang, C.P. (2001), "Finite layer method in analysis of piezoelectric composite laminates", *Comput. Method. Appl. Mech. Eng.*, **191**(8-10), 879-901.

Cheung, Y.K. and Kong, J. (1993), "Approximate three-dimensional analysis of rectangular thick laminated plates: bending, vibration and buckling", *Comput. Struct.*, **47**(2), 193-199.

D'Ottavio, M. and Carrera, E. (2010), "Variable-kinematics approach for linearized buckling analysis of laminated plates and shells", *AIAA J.*, **48**(9), 1987-1996.

Fan, J. and Ye, J. (1993), "Exact solutions of buckling for simply supported thick laminates", *Compos. Struct.*, **24**(1), 23-28.

Gu, H. and Chattopadhyay, A. (2000), "Three-dimensional elasticity solution for buckling of composite laminates", *Compos. Struct.*, **50**(1), 29-35.

Kim, S.E., Thai, H.T. and Lee, J. (2009a), "Buckling analysis of plates using the two variable refined plate theory", *Thin Wall. Struct.*, **47**(4), 455-462.

Kim, S.E., Thai, H.T. and Lee, J. (2009b), "A two variable refined plate theory for laminated composite plates", *Compos. Struct.*, **89**(2), 197-205.

Na, K.S. and Kim, J.H. (2004), "Three-dimensional thermal buckling analysis of functionally graded materials", *Compos. Part B - Eng.*, **35**(5), 429-437.

Na, K.S. and Kim, J.H. (2006), "Three-dimensional thermomechanical buckling analysis for functionally graded composite plates", *Compos. Struct.*, **73**(4), 413-422.

Nali, P., Carrera, E. and Lecca, S. (2011), "Assessments of refined theories for buckling analysis of laminated plates", *Compos. Struct.*, **93**(2), 456-464.

Noor, A.K. (1975), "Stability of multilayered composite plates", *Fibre Sci. Technol.*, **8**(2), 81-89.

Noor, A.K., Burton, W.S. (1990), "Assessment of computational models for multilayered anisotropic plates", *Compos. Struct.*, **14**(3), 233-265.

Noor, A.K., Burton, W.S. and Bert, C.W. (1996), "Computational model for sandwich panels and shells", *Appl. Mech. Rev.*, **49**, 155-199.

Reddy, J.N. (1993), "An evaluation of equivalent single layer and layerwise theories of composite laminates", *Compos. Struct.*, **25**, 21-35.

Reddy, J.N. and Khdeir, A.A. (1989), "Buckling and vibration of laminated composite plates using various plate theories", *AIAA J.*, **27**(12),1808-1817.

Reddy, J.N. and Phan, N.D. (1985), "Stability and vibration of isotropic, orthotropic and laminated plates according to a higher-order shear deformation theory", *J. Sound Vib.*, **98**(2), 157-170.

Reissner, E. (1984), "On a certain mixed variational theory and a proposed application", *Int. J. Numer Meth. Eng.*, **20**, 1366-1368.

Reissner, E. (1986a), "On a mixed variational theorem and on a shear deformable plate theory", *Int. J. Numer Meth. Eng.*, **23**(6), 193-198.

Reissner, E. (1986b), "On a certain mixed variational theorem and on laminated elastic shell theory", *Proc. Euromech-Colloquium*, **219**, 17-27.

Teo, T.M. and Liew, K.M. (1999a), "Three-dimensional elasticity solutions to some orthotropic plate problems", *Int. J. Solids Struct.*, **36**(3-4), 5301-5326.

Teo, T.M. and Liew, K.M. (1999b), "A differential quadrature procedure for three-dimensional buckling analysis of rectangular plates", *Int. J. Solids Struct.*, **36**(8), 1149-1168.

Thai, H.T., Kim, S.E. (2011), "Levy-type solution for buckling analysis of orthotropic plates based on two variable refined plate theory", *Compos. Struct.*, **93**(7), 1738-1746.

Wu, C.P. and Chang, R.Y. (2012), "A unified formulation of RMVT-based finite cylindrical layer methods for sandwich circular hollow cylinders with an embedded FGM layer", *Compos. Part B - Eng.*, **43**(8), 3318-3333.

Wu, C.P. and Chen, C.W. (2001), "Elastic buckling of multilayered anisotropic conical shells", *J. Aerospace Eng.*, **14**(1), 29-36.

Wu, C.P. and Chen, W.Y. (1994), "Vibration and stability of laminated plates based on a local high order plate theory", *J. Sound Vib.*, **177**(4), 503-520.

Wu, C.P., Chiu, K.H. and Wang, Y.M. (2008), "A review on the three-dimensional analytical approaches of multilayered and functionally graded piezoelectric plates and shells", *Comput. Mater. Continua*, **18**, 93-132.

Wu, C.P. and Chiu, S.J. (2001), "Thermoelastic buckling of laminated composite conical shells", *J. Therm. Stresses*, **24**(9), 881-901.

Wu, C.P. and Chiu, S.J. (2002), "Thermally induced dynamic instability of laminated composite conical shells", *Int. J. Solids Struct.*, **39**(11), 3001-3021.

Wu, C.P. and Li, H.Y. (2010), "The RMVT- and PVD-based finite layer methods for the three-dimensional analysis of multilayered composite and FGM plates", *Compos. Struct.*, **92**(10), 2476-2496.

Wu, Z., Chen, W. (2007), "Thermomechanical buckling of laminated composite and sandwich plates using global-local higher order theory", *Int. J. Mech. Sci*., **49**(6), 712-721.

Wu, Z. and Chen, W. (2008), "An assessment of several displacement-based theories for the vibration and stability analysis of laminated composite and sandwich beams", *Compos. Struct*., **84**(4), 337-349.

Wu, Z., Cheung, Y.K., Lo, S.H., Chen, W. (2008), "Effects of higher-order global-local shear deformations on bending, vibration and buckling of multilayered plates", *Compos. Struct*., **82**(2), 277-289.

Zenkour, A.M. (2005), "A comprehensive analysis of functionally graded sandwich plates: Part 2-Buckling and free vibration", *Int. J. Solids Struct.* **42**, 5243-5258.

Zenkour, A.M., Ai-Sheikh, K. (2001), "Buckling and free vibration of elastic plates using simple and mixed shear deformation theories", *Acta Mech*., **146**(3-4), 183-197.

Zenkour, A.M. and Fares, M.E. (2001), "Bending, buckling and free vibration of non-homogeneous composite laminated cylindrical shells using a refined first-order theory", *Compos. Part B - Eng*., **32**(3), 237-247.

Zhao, X., Lee, Y.Y. and Liew, K.M. (2009), "Mechanical and thermal buckling analysis of functionally graded plates", *Compos. Struct*., **90**(2), 161-171.

CC